Journal of Catalysis 284 (2011) 184–193

Contents lists available at SciVerse ScienceDirect

Journal of Catalysis

journal homepage: www.elsevier.com/locate/jcat

Selective and regular localization of accessible Pt nanoparticles inside the walls of an ordered silica: Application as a highly active and well-defined heterogeneous catalyst for propene and styrene hydrogenation reactions

M. Boualleg [a], S. Norsic [a], D. Baudouin [a], R. Sayah [a], E.A. Quadrelli [a], J.-M. Basset [a,1], J.-P. Candy [a], P. Delichere [b], K. Pelzer [c,2], L. Veyre [a], C. Thieuleux [a,*]

[a] Université de Lyon, Institut de Chimie de Lyon, UMR 5265 – CNRS – Université Lyon 1, ESCPE Lyon, Laboratoire de Chimie, Catalyse, Polymères et Procédés (C2P2), Equipe Chimie Organométallique de Surface, 43, Bd du 11 Novembre 1918 F-69616 Villeurbanne, France
[b] Université de Lyon, Institut de Chimie de Lyon, UMR 5256 – CNRS – Université de Lyon 1, Institut de Recherches sur la Catalyse et l'Environnement de Lyon (IRCELyon), 2 avenue A. Einstein F-69616 Villeurbanne, France
[c] Fritz-Haber-Institutes of the Max Planck Society, Department for Inorganic Chemistry, Faradayweg 4-6, 14195 Berlin, Germany

ARTICLE INFO

Article history:
Available online 26 October 2011

Keywords:
Platinum
Nanoparticles
Colloids
Mesoporous materials
Hydrogenation
Heterogeneous catalysis

ABSTRACT

We describe here an original methodology related to the "build-the-bottle-around-the-ship" approach yielding a highly ordered silica matrix containing regularly distributed Pt nanoparticles (NPs) located inside the silica walls, **Pt@{walls}SiO_2**. The starting colloidal solution of crystalline Pt nanoparticles was obtained from $Pt(dba)_2$ (dba = dibenzylidene acetone) and 3-chloropropylsilane. The resulting nanoparticles (diameter: 2.0 ± 0.4 nm determined by HRTEM) resulted hydrophilic. The NPs present in the THF colloidal solution were incorporated inside the walls of a highly ordered 2D hexagonal mesoporous silica matrix via sol–gel process using a templating route with tetraethylorthosilicate, TEOS, as the silica source, and block copolymer $(EthyleneOxide)_{20}(PropyleneOxide)_{70}(EthyleneOxide)_{20}$ (Pluronic P123) as the structure-directing agent. Low-temperature calcination of the crude material at 593 K led to the final solid **Pt@{walls}SiO_2**. Characterization by IR, HRTEM, BF-STEM and HAADF-STEM, SAXS, WAXS, XRD, XPS, H_2 chemisorption, etc. of **Pt@{walls}SiO_2** confirmed the 2D hexagonal structuration and high mesoporosity (870 m^2/g) of the material as well as the presence of stable 2-nm-sized crystalline Pt(0) NPs embedded inside the walls of the silica matrix. The material displayed no tendency to NPs sintering or leaching (Pt loading 0.3 wt.%) during its preparation.

Pt@{walls}SiO_2 was found to be a stable, selective and highly active hydrogenation catalyst. The catalytic performances in propene hydrogenation were tested under chemical regime conditions in a tubular flow reactor (278 K, propene/H_2/He = 20/16/1.09 cm^3/min, P_{tot} = 1 bar) and were found superior to those of an homologous solid containing Pt NPs along its pore channels **Pt@{pores}SiO_2** and to those of a classical industrial catalysts **Pt/Al_2O_3**, (TOF = 2.3 s^{-1} vs. TOF = 0.90 and 0.92 s^{-1}, respectively, calculated per surface platinum atoms). **Pt@{walls}SiO_2** also catalyzes fast and selective styrene hydrogenation. A material containing by design Pt NPs both in its walls and in its pores, **Pt@{walls + pores}SiO_2**, is also described.

1. Introduction

Several classical techniques are used in industry for the synthesis of materials containing metal nanoparticles, with applications in numerous fields among which is catalysis [1–3]. A recurrent drawback of these preparative routes is that the materials display metallic nanoparticles randomly dispersed, with little control over their localization, size or strength of the interaction with the solid.

As recently reviewed [4–6], several strategies have been developed to circumvent such lack of control. The routes relying on the decomposition of organometallic complexes are among the most successful approaches for localization of the nanoparticles *inside the walls* of the support, that is embedded inside the support's framework; such routes have led, for example, to the selective localization of the metal nanoparticles inside the walls of mesostructured silicas [7–10] or of hybrid organic–inorganic materials [11].

* Corresponding author.
E-mail address: thieuleux@cpe.fr (C. Thieuleux).
[1] Present address: Catalysis Research Center, King Abdullah University of Science and Technology, Jeddah, Saudi Arabia.
[2] Present address: Laboratoire Chimie Provence UMR 6264, Université d'Aix-Marseille I, Bâtiment Madirel, Campus St. Jérôme, 13397 Marseille Cedex 20, France.

0021-9517/$ - see front matter © 2011 Elsevier Inc. All rights reserved.
doi:10.1016/j.jcat.2011.09.003

A different recent strategy to highly ordered oxide matrixes containing metal nanoparticles localized preferentially *in the pores*, i.e. deposited on the surface of the oxides' pores, consists in the *in situ* controlled synthesis of mesostructured materials around preformed nanoparticles [12–17], comparable to the "build-the-bottle-around-the-ship" synthesis of zeolitic materials around preformed complexes [18]. Such "build-the-bottle-around-the-ship" approach applied to mesoporous silicas around preformed nanoparticles generally leads to a very good control over the nanoparticle size and over the regularity of the NPs distribution throughout the material's mesopores. For example, using this methodology, we synthesized mesostructured silicas with regularly distributed 2–3.5-nm Pt(0) nanoparticles in their pores, **Pt@{pores}SiO_2**, which proved to be highly active and long lived in propene hydrogenation [17]. We attribute the success of the strategy for a big part in designing preformed nanoparticles whose size, structure and chemical nature are tailored for excellent compatibility with the sol–gel process and with the template removal step. Specifically, the hydrophobicity of the nanoparticles, conferred by the presence of alkylsilane ligands around the preformed platinum nanoparticles, allowed the localization of the NPs inside the hydrophobic core of the surfactant micelle. The presence of the nanoparticles in the core of the micelle led to NPs regularly distributed in the pores of the materials. Such methodology is therefore inherently limited to NPs smaller than the ultimate size of the micelles (and thereby of the silica pores) and to nanoparticles located in the pores and systematically absent from the walls of the material.

We describe herein an original methodology related to such "build-the-bottle-around-the-ship" approach. Our methodology yields a highly mesostructured material containing regularly distributed, fully accessible and stable 2-nm Pt(0) nanoparticles systematically absent from the pores and exclusively located *inside the walls* (i.e. embedded inside the silica matrix), **Pt@{walls}SiO_2**, that is to say having the reverse localization with respect to our previously reported **Pt@{pores}SiO_2** [17]. The selective localization of accessible Pt(0) nanoparticles inside the walls instead of in the pores is expected to improve their thermal and chemical stability as well as their catalytic performances. The accessibility to the embedded NPs will be granted by the network of microporous channels (that is a network of channels of diameter of <2 nm) present inside the silica walls (typically 7 nm thick). If such network of micropores did not exist, the NPs would result inaccessible because occluded inside the matrix, the material would be thus catalytically inactive. Some examples of accessible NP selectively localized inside the walls of mesostructured oxides can be found [7–9,19,20]. In some cases, the above-mentioned decomposition of organometallic complexes in the micropores of preformed oxides is achieved via a multi-step methodology, which requires a specific tuning for each metal, while providing limited control over the metal nanoparticles (NPs) size and localization [7–9]. In some other cases, preformed metal nanoparticles, like in our case, are implied [19,20]. These latter literature examples generally lead to embedded oxidized metals (e.g., CeO_2, ZrO_2, TiO_2, Al_2O_3, AlO(OH), La_2O_3, Fe_2O_3, or Fe_3O_4) and are therefore suited for applications linked to their magnetic or other physical properties rather than catalytic applications requiring reduced metals, such as the proof-of-concept hydrogenations discussed herein.

2. Experimental

2.1. Materials and methods

Dibenzylidene acetone (dba), potassium tetrachloroplatinate salt (K_2PtCl_4-97%), block copolymer $(EthyleneOxide)_{20}(PropyleneOxide)_{70}(EthyleneOxide)_{20}$ (Pluronic P123), silicon carbide (SiC) and sodium fluoride (NaF – 99%) were purchased from Aldrich and used as received. Butylsilane (97%) and 3-chloropropyltriethoxysilane were purchased from ABCR and used as received. Tetraethylorthosilicate (TEOS, 98%, Aldrich) was dried on magnesium powder and further distilled under argon overnight prior to use. Synthesis of the platinum nanoparticles and of 3-chloropropyltrihydrogenosilane are described in SI. Material **Pt@{pores}SiO_2** was synthesized as previously reported [17]. Commercial **Pt@Al_2O_3** (0.32 wt.%, metal dispersion 70–80%) was generously provided by AXENS (France).

Propene (Alphagaz 1, Air Liquide), He (Alphagaz 1, Air Liquide) and H_2 were purified over R3–11 BASF catalyst/MS 4 Å prior to use. $Pt(dba)_2$ complex was prepared as previously reported [21]. THF and Pentane were distilled, respectively, on benzophenone and NaK under Ar.

The analytical procedures, performed on the equipments below, are described in the SI.

Elemental analysis: Elemental analyses were performed at the "Laboratoire de Synthèse et d'Electrosynthèse Organométallique", UMR 5188 CNRS, Dijon, France and at the service "Service Central d'Analyses" of the CNRS in Vernaison, France.

Transmission Electron Microscopy (TEM): *Conventional TEM micrographs* for analyzing the Pt NPs colloids were performed at the "Centre Technologique des Microstructures", UCBL, Villeurbanne, France, using a Philips CM120 electron microscope. The acceleration voltage was 120 kV. *High-Resolution TEM micrographs* were performed at the Fritz-Haber-Institute of the Max Planck Society of Berlin, Germany, on a Philips CM200 Transmission Electron Microscope. The acceleration voltage was 200 kV. *STEM (HAADF and BF) micrographs* were performed at the "Institut de Recherche sur la Catalyse et l'Environnement de Lyon", IRCELyon CNRS, Villeurbanne, France on a Jeol 2010 Transmission Electron Microscope. The acceleration voltage was 200 kV.

Wide-Angle X-ray Scattering (WAXS): The data collection for the wide-angle X-ray scattering was performed at CEMES, Toulouse, France on a SEIFERT XRD apparatus. Time for data collection was typically for a set of 457 measurements collected at room temperature in the range of: $0° < \theta < 65°$.

Small-Angle X-ray Diffraction (XRD): XRD measurements were carried out with a Rigaku D/max-r C diffractometer (40 kV, 50 mA) with Cu Kα radiation (λ = 0.154 nm) in the "Centre de diffractometrie H. Longchambon", Université de Lyon, Lyon, France.

X-ray Photoelectron Spectroscopy: XPS measurements were performed at the Institut de Recherche sur la Catalyse et l'Environnement de Lyon, IRCELyon CNRS, Villeurbanne, France using a KRATOS Axis Ultra DLD spectrometer.

H_2 Chemisorption adsorption measurements were performed on a BELSORB-max from BEL JAPAN.

Nitrogen adsorption/desorption measurements were performed at 77 K. The N_2 adsorption/desorption measurements were carried out using an ASAP 2020 Micromeritics system. Before N_2 adsorption, the samples were outgassed at 10^{-4} Pa at 573 K for 2 h.

GC analyses: Gas phase analyses for propene hydrogenation were performed on a Hewlett Packard 5890 series II gas chromatography (GC) apparatus equipped with a flame ionization detector (FID) and a KCl/Al_2O_3 column (50 m × 0.32 mm). Liquid phase analyses for styrene hydrogenation were performed on a Hewlett Packard 6890 series gas chromatography (GC) apparatus equipped with a flame ionization detector (FID) and a Bentone® column (50 feet × 0.32 in.).

Infrared spectroscopy: *The Diffuse Reflectance Infrared Fourier Transform (DRIFT) spectra* of solid compounds were collected from a Nicolet FT-IR Spectrometer equipped with a MCT detector. The laser impinging the sample surface is a helium/neon type with 632.8 nm of wavelength. Before use, liquid azote was introduced onto the machine for cooling devices. *The transmission spectra of*

liquid samples were obtained using a Nicolet FT-IR Spectrometer equipped with a DTGS detector; 32 scans per sample were recorded, averaged for each spectrum and corrected against the spectrum with KBr or ambient air as background in the case of liquid and solid samples, respectively.

2.2. Preparation of the Pt NPs-containing materials

2.2.1. Pt NPs located inside the walls of the silica matrix, ***Pt@{walls}SiO$_2$***

The material containing Pt NPs inside its walls was prepared by contacting the THF solution of Pt nanoparticles **Pt—Cl$_{silane}$** (12 mL, 17.9 μmol of Pt) with an aqueous solution of Pluronic P123 surfactant (0.5 g of P123 in 50 mL of deionized water) and a catalytic amount of NaF (0.02 g, 0.47 mmol). Simultaneously, an acidic aqueous solution (0.17 g of HCl, 37%, 5 ml of deionized water) of TEOS (5 g, 24 mmol) was prepared and stirred for 2 h at 35 °C. After the slow evacuation of the THF from the NPs-containing solution, the silicate solution was added to the latter, and the resulting mixture was stirred for 48 h at 35 °C. The resulting deep gray precipitate (yield: 95%) was filtered off, washed with water, ethanol and ether and finally dried under vacuum (10^{-5} mbar) at 400 K for 15 h to yield the as-synthesized solid **Pt@{walls}SiO$_{2\text{-crude}}$**.

Elemental analyses (wt.%) : Found : Pt = 0.22 ± 0.05,
Si = 39.35 ± 0.05

See main text and SI for WAXS data.

The crude product **Pt@{walls}SiO$_{2\text{-crude}}$** (1 g batch per calcination) was calcined in a Pyrex tubular reactor under dry air at 593 K (heating slope 2 K/min, 10 h) to yield the final product **Pt@{walls}SiO$_2$**.

Elemental analyses (wt.%) : C ⩽ 0.1; Cl = 0; Pt = 0.30 ± 0.05,
Si = 41.00 ± 0.05.
N_2adsorption/desorption : Surface area (BET)
: 1050 m^2/g (micropores 465 m^2/g).
Pore size distribution : mesopores (BJH) : 7 nm.
Micropores (HK) : 1 nm.

See Section 3 for XRD, SAXS, HRTEM data. IR (DRIFT), WAXS, XPS data, H_2 chemisorption and propene adsorption measurements are reported in SI.

The as-synthetized material **Pt@{walls}SiO$_{2\text{-crude}}$** (1 g batch) was also Soxhlet extracted in hot ethanol to yield the product **Pt@{walls}SiO$_{2\text{-extract}}$**.

N_2 adsorption/desorption: Surface area (BET) 601 m^2/g; micropores 97 m^2/g. See main text for results in styrene hydrogenation.

2.2.2. Pt NPs located both in the pores and in the walls of the silica matrix, ***Pt@{walls + pores}SiO$_2$***

The material containing Pt NPs in its pores and walls was prepared by merging the two above-mentioned THF solutions of Pt NPs **Pt—Cl$_{silane}$** and **Pt—But$_{silane}$** in a 1:1 molar ratio (final volume 24 mL, total Pt content 35.8 μmol) with an aqueous solution of Pluronic P123 surfactant (0.5 g of P123 in 50 mL of deionized water) and a catalytic amount of NaF (0.02 g, 0.47 mmol). An acidic solution (0.17 g of HCl, 37%, 5 ml of deionized water) of TEOS (5 g, 24 mmol) was prepared and stirred for 2 h at 35 °C. After the slow evacuation of the THF from the NPs solutions, the silicate solution was added to the NPs solution, and the resulting mixture was stirred for 48 h at 35 °C. The resulting deep gray precipitate was filtered off, washed with water, ethanol and ether and finally dried under vacuum (10^{-5} mbar) at 400 K for 15 h. The elemental analysis of this as-synthesized solid **Pt@{walls + pores}SiO$_{2\text{-crude}}$** shows the quantitative incorporation of the Pt nanoparticles (found: 0.60 ± 0.05 wt.%).

The crude product **Pt@{walls + pores}SiO$_{2\text{-crude}}$** (1 g batch per calcination) was calcined in a Pyrex tubular reactor under dry air at 593 K (heating slope 2 K/min, 10 h) to yield the final product **Pt@{walls + pores}SiO$_2$**.

See SI for TEM micrographs.

2.2.3. Pt-free silica matrix, ***blank-SiO$_2$***

The platinum-free homologous material, **blank-SiO$_2$**, was synthesized according to the procedures above by replacing the colloidal THF solution by pure THF. A calcination at 723 K was performed to completely remove the template. See Section 3, for N_2 adsorption/desorption and SI for propene adsorption data.

2.3. Propene hydrogenation in a flow reactor

Materials **Pt@{walls}SiO$_2$**, **Pt@{walls}SiO$_{2\text{-extract}}$**, **Pt@{pores}-SiO$_2$** and **Pt/Al$_2$O$_3$** were tested as catalysts in propene hydrogenation reaction in a tubular flow reactor. Preliminary experiments to ensure the chemical regime during the measurements are described in main text (see SI for figures).

2.3.1. Representative standard procedure

The catalyst containing 0.3 wt.% of Pt (7 mg, 0.107 μmol of Pt) was closely mixed in SiC (900 mg), and the loose powder was loaded in a fixed-bed glass flow reactor. The isolated reaction chamber was flushed with helium for 1 h, and the solid was further treated under H_2 for 3 h at 573 K. After cooling to 278 K, the reactor was connected to the propene/H_2/He line (20/16/1.09 cm^3/min) and the pressure was set to 1 bar. The opening of the valve corresponds to the beginning of the catalytic test (t = 0). The progress of the reaction was monitored by GC using an auto-sampler.

2.4. Styrene hydrogenation of in a pressurized batch reactor

Materials **Pt@{walls}SiO$_2$** and **Pt@Al$_2$O$_3$** were tested as catalysts for styrene hydrogenation reaction in batch conditions as described below.

Representative procedure: The Pt catalyst [150 mg, 2.3 μmol of Pt, viz. 0.92 μmol of $Pt_{surface}$ (40% dispersion) for **Pt@{walls}SiO$_2$** and 1.96 mol of $Pt_{surface}$ for **Pt/Al$_2$O$_3$** (75% dispersion)], styrene [9862 μmol, i.e., 10,000 equiv. per $Pt_{surface}$ for **Pt@{walls}SiO$_2$** and 5000 equiv. per $Pt_{surface}$ for **Pt/Al$_2$O$_3$**] and heptane (50 mL) were loaded in a 100-mL pressurized batch reactor in the glove box. The reaction mixture was put under vigorous stirring and pressurized with 35 bars of H_2. The pressure in the reactor was kept at 35 ± 4 bars, while small aliquots of the solution were drawn and analyzed by GC to monitor the reaction.

2.5. Propene adsorption measurements

Propene adsorption by materials **Pt@{walls}SiO$_2$**, **Pt@Al$_2$O$_3$** and **blank-SiO$_2$** was carried out at 278 K using a conventional Pyrex volumetric adsorption equipment. The vacuum (10^{-6} mbar) was achieved with a liquid nitrogen-trapped mercury diffusion pump. The equilibrium pressure was measured with a Texas Instrument gauge (pressure range, 0–1000 mbar with an accuracy of 0.1 mbar). The catalyst sample was loaded in a Pyrex cell and outgassed at 298 K and then at 573 K for 3 h under vacuum (see SI for figures).

3. Results and discussion

3.1. Synthesis and characterization of the materials

The targeted ordered oxides containing platinum nanoparticles inside either the walls, **Pt@{walls}SiO_2**, or both in the pores and in the walls, **Pt@{walls + pores}SiO_2**, were prepared in a quantitative yield by the controlled growth of a highly ordered silica matrix around platinum colloids, **Pt—Cl_{silane}** or a mixture of **Pt—Cl_{silane}** and **Pt—But_{silane}**, respectively. The experimental procedure consisted of two steps: (1) the synthesis of a colloidal solution of small Pt nanoparticles stabilized by a non-exchangeable silylated ligand (3-chloropropylsilane for **Pt—Cl_{silane}** and butylsilane for **Pt—But_{silane}**), (2) the growth of a mesostructured silica matrix with adequate walls for incorporating the nanoparticles using a sol–gel process via a templating route followed by the elimination of the organics (surfactant and silane ligands) from the materials to render the embedded NPs accessible during the catalytic tests. A special effort was dedicated to fully control and characterize by advanced techniques each step leading to the final material.

3.1.1. Step 1: Synthesis and characterization of the Pt colloidal solutions, *Pt—Cl_{silane}* and *Pt—But_{silane}*

The colloidal solution of Pt nanoparticles **Pt—Cl_{silane}** was prepared using an experimental procedure developed in the laboratory for the synthesis of metal nanoparticles using alkylsilane as the stabilizing ligands [17,22,23]. Here, the procedure was applied with $Pt(dba)_2$ as the metal source, 3-chloropropylsilane (0.5 eq. with respect to Pt) as the stabilizing ligand and THF as the polar solvent. As in the previous cases, the resulting solution exhibits a narrow range of nanoparticles sizes centered at 1.8 ± 0.4 nm according to TEM micrographs (Fig. 1).

The IR spectrum of the platinum nanoparticles stabilized with the chlorinated silane precursor, **Pt—Cl_{silane}**, displays the characteristic bands of alkyl —CH_2 groups between 2800 and 3000 cm^{-1} (see Fig. S2). The absence of the stretching ν(Si—H) band of the starting silane at 2154 cm^{-1} indicates the loss of hydrogen during the grafting of Si on the Pt surface. In analogy with similar results observed for homologous procedures for Pt [17,24] or Ru [22] NPs preparation using octylsilane as stabilizing ligand, the infrared evidence on **Pt—Cl_{silane}** nanoparticles suggests the existence of ≡Si(n-C_3H_6Cl) fragments grafted on the metal surface.

The nanoparticles **Pt—Cl_{silane}** are hydrophilic: addition of an aliquot of the THF colloidal suspension of **Pt—Cl_{silane}** to 1: 1 water: heptane mixture results in a black coloration of the aqueous phase. When the experiment is repeated with the nanoparticles **Pt—But_{silane}** obtained with the n-butylsilane rather than 3-chloropropylsilane as stabilizing ligands or with the already reported **Pt—Oct_{silane}**, the nanoparticles are in the organic phase and are hence hydrophobic (Fig. 2). Thus, the 3-chloropropylsilane ligand seems to be sufficient to switch the polar character of **Pt—Cl_{silane}** nanoparticles from hydrophobic to hydrophilic. A possible explanation could be the terminal carbon–chloride bond polarization in polar solvents [25].

3.1.2. Step 2 for the material containing Pt NPs inside the walls *Pt@{walls}SiO_2*: Preparation and characterization

The mesophasis leading to material **Pt@{walls}SiO_2** was obtained by contacting at 35 °C the hydrophilic Pt NPs colloidal solution **Pt—Cl_{silane}** and an aqueous solution of Pluronic P123 containing a catalytic amount of NaF (needed for the further condensation of silicates during the sol–gel process). THF was chosen as the solvent for Pt NPs colloidal solution because of its polar character (ensuring the dispersion of the NPs in the polar surfactant/water mixture) and its compatibility as a co-solvent for materials synthesis [26]. After 2 h under stirring, slow evacuation of THF was performed to reduce its volume to less than 1 mL (maximum volume acceptance for no disruption of the surfactant mesophasis). No aggregation of the Pt nanoparticles was observed. In parallel, an acidic solution of tetraethylorthosilicate, TEOS, was prepared and stirred during 2 h at 35 °C in order to prehydrolyze the TEOS into silicates. The latter solution was further rapidly added to the

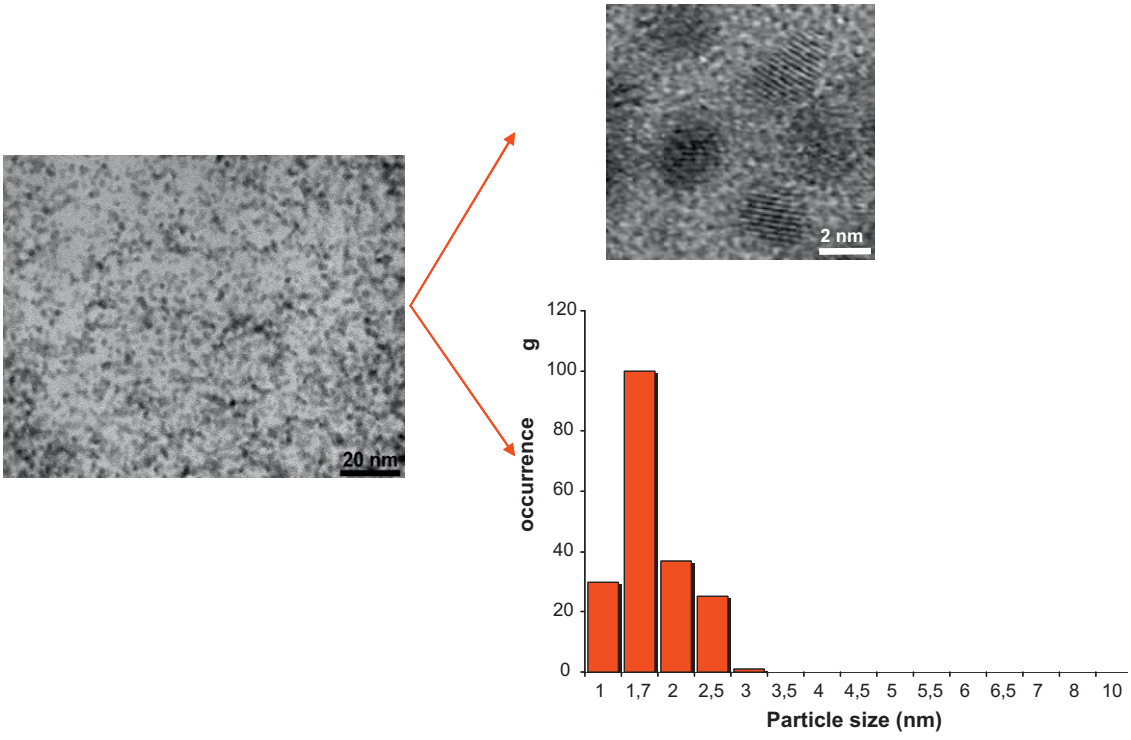

Fig. 1. TEM (left) and HRTEM (top right) micrograph and size histogram (bottom right) of the THF colloidal solution of Pt nanoparticles **Pt—Cl_{silane}**.

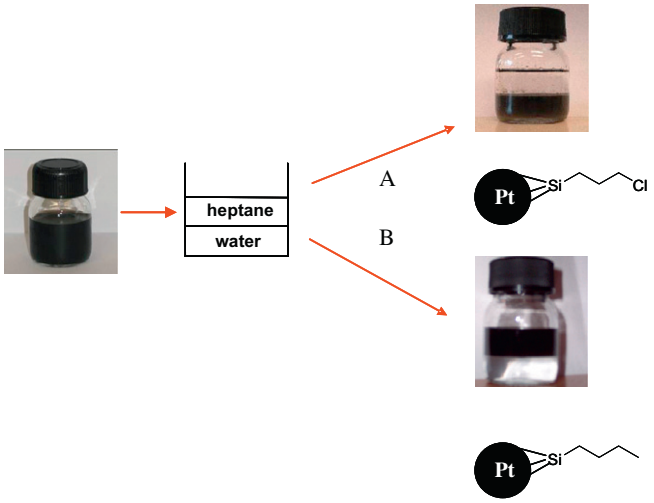

Fig. 2. Pictures of the water/heptane mixture containing the Pt nanoparticles stabilized by (A) the 3-chloropropylsilane ligands, **Pt—Cl$_{silane}$** and (B) the n-butylsilane ligands, **Pt—But$_{silane}$**.

NPs/surfactant solution at 35 °C, and a gray precipitate **Pt@{walls}SiO$_{2\text{-crude}}$** was immediately formed. The above procedure was repeated over 10 times with fully reproducible results. This experimental protocol was inspired from that of Jin et al. [27] and allowed generating silica materials having (i) an important wall thickness of ca. 7 nm (superior to the estimated 4 nm size of the stabilized Pt nanoparticles) to insure the full incorporation of the nanoparticles inside the walls and (ii) microporous channels through out the silica walls that allow the accessibility of the embedded nanoparticles inside the material's walls in view of the catalytic applications, which require substrate access to the active site.

The elemental analysis of the as-synthesized material **Pt@{walls}SiO$_{2\text{-crude}}$** recovered after filtration and gentle drying indicated a Pt/Si molar ratio of 7.5×10^{-4} (Pt = 0.22 wt.%). This Pt/Si ratio is substantially equal to the calculated Pt/Si molar ratio of 8.0×10^{-4} present in the starting TEOS/Pt colloid solution **Pt—Cl$_{silane}$**/surfactant system, thus showing the quantitative incorporation of the Pt nanoparticles present in the colloid solution into the material **Pt@{walls}SiO$_{2\text{-crude}}$**. The size of the crystallites (2 nm) in **Pt@{walls}SiO$_{2\text{-crude}}$** measured by Wide-Angle X-ray Scattering (WAXS) (see SI – Fig. S3) is substantially identical to the starting size of the Pt NP in the starting colloid **Pt—Cl$_{silane}$** showing that no colloid disruption has occurred during the sol–gel process.

The surfactant and the solvent were removed from **Pt@{walls}SiO$_{2\text{-crude}}$** by gentle (Soxhlet) solvent extraction. The resulting solid **Pt@{walls}SiO$_{2\text{-extract}}$** (see SI) retains substantially all the platinum initially introduced, showing that no leaching occurs upon solvent extraction. This behavior is markedly different from the analogous material **Pt@{pores}SiO$_{2\text{-extract}}$** synthesized from hydrophobic **Pt—Oct$_{silane}$** colloids, for which Soxhlet extraction induced nanoparticles leaching [17]. We attribute this different behavior between **Pt@{walls}SiO$_{2\text{-extract}}$** and **Pt@{pores}SiO$_{2\text{-extract}}$** toward metal leaching during Soxhlet extraction to the embedding of the nanoparticles inside the walls of the matrix in the former material. The embeddedment is thought to protect against leaching during contact with hot solvent, while the same treatment washes away the NPs present in the pores in the latter material. The textural properties of the material **Pt@{walls}SiO$_{2\text{-extract}}$** (surface area 601 m^2/g; microporosity 97 m^2/g) show that the extraction protocol does not fully liberate the microporosity of the walls, which can be as high as 465 m^2/g in an analogous calcined (rather than extracted) material (see below).

Therefore, albeit useful for indicating the actual embedding of the NPs inside the walls, this extraction method is not the method of choice for yielding ordered silica matrixes containing fully accessible metal nanoparticles inside the walls, where the accessibility is a necessary requisite for catalysis (see below for the poor catalytic performances of **Pt@{walls}SiO$_{2\text{-extract}}$** in propene hydrogenation). A low-temperature calcination treatment (593 K) was therefore chosen for **Pt@{walls}SiO$_{2\text{-crude}}$** activation. Elemental analyses on the final material **Pt@{walls}SiO$_2$** (C < 0.1 wt.%, no Cl detected) indicate that such treatment quantitatively evacuates the surfactant and chloropropyl chains of the stabilizing silane ligands. The IR spectrum of the calcined material, which is dominated by the ν(OH) at ca. 3700 cm^{-1} and the deformation mode of the siloxy framework below 2000 cm^{-1}, displays hardly any ν(C—H) between 2800 and 3000 cm^{-1}, confirming a complete removal of the organic ligand and the surfactant (see SI – Fig. S3).

The metal loading in the calcined solid **Pt@{walls}SiO$_2$** (0.30 wt.%, which corresponds to 3.4 ± 0.6 mgPt/gSiO_2) is also coherent with the successful removal of organics from **Pt@{walls}-SiO$_{2_crude}$** (0.22 wt.%, 2.6 ± 0.6 mgPt/gSiO_2) and retention of all the metal. Therefore, no metal leaching occurred upon calcination of **Pt@{walls}SiO$_{2\text{-crude}}$**.

N_2 adsorption/desorption measurements of the final material **Pt@{walls}SiO$_2$** exhibited an isotherm of type IV corresponding to a mesoporous material and confirmed the complete removal of the surfactant in both mesopores and micropores (BET surface area of 1050 m^2/g with 465 m^2/g of micropores as given by t-plot method), as well as the presence of narrow mesopore and micropore size distributions centered, respectively, at 7 nm (using BJH method at the adsorption branch) and 1 nm (using HK method) (Fig. 3). The reference material **blank-SiO$_2$** (i.e. highly structured silica homologous to **Pt@{walls}SiO$_2$** without Pt nanoparticles) exhibited texture and structuration properties (surface area of 795 m^2/g with a microporous surface area of 335 m^2/g, mesopore and micropore size distributions centered, respectively, at 6 nm and 1 nm, Fig. 3) that are comparable to those of the platinum-containing solid **Pt@{walls}SiO$_2$**. The X-ray Diffraction pattern of **Pt@{walls}SiO$_2$** (Fig. 3) displayed the characteristic peaks of a 2D hexagonal long-range ordering of the channel pores with a wall thickness estimated at 7 nm.

The High-Resolution Transmission Electron Microscopy (HRTEM) micrographs reported in Fig. 4 on an ultra fine slice of the coated sample show the presence of parallel pore channels in the sample. When zooming to a 20-nm scale (Fig. 4B and C), the hexagonal arrangement of the pore channels can be observed (presence of a honeycomb structure in Fig. 4B and parallel channels in Fig. 4C). Small Pt nanoparticles (2 nm) located inside the walls of the silica matrix (as highlighted by the arrows) are also visible on the micrographs.

The size of the Pt crystallites located inside the walls of **Pt@{walls}SiO$_2$** was measured by WAXS at 2.0 ± 0.4 nm (see Fig. S4). H_2 chemisorption measurement on the platinum nanoparticles of the final material **Pt@{walls}SiO$_2$** estimated a dispersion of *ca.* 40%, i.e., a mean size particle diameter of 2.6 ± 0.4 nm (see Fig. S5, this calculation was performed taking into account a chemisorptions of 1.7H per Pt surface atom [28]). Such chemisorption measurements also indirectly show that the surface of the nanoparticles is not covered by carbonaceous compounds, which can be a known undesirable side-effect of calcinations.

In summary, data provided by WAXS, TEM and H_2 chemisorption show that the size of the Pt NPs present in the final material **Pt@{walls}SiO$_2$** (ca. 2 nm diameter) is substantially identical to NP size in the as-synthetized material **Pt@{walls}SiO$_{2\text{-crude}}$**, indicating that no sintering occurs upon calcination. The complete retention of

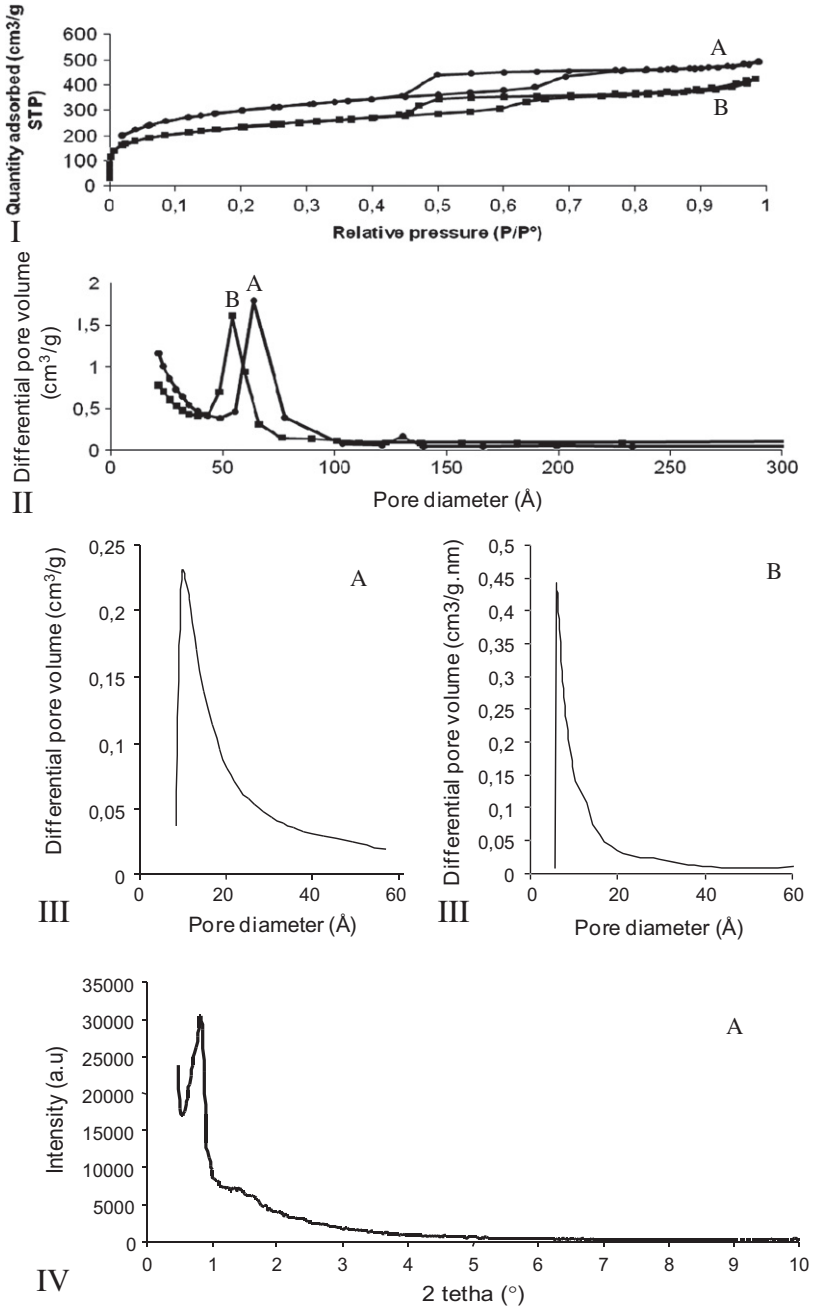

Fig. 3. Physical characteristics of (A) the material containing Pt nanoparticles inside the walls **Pt@{walls}SiO$_2$**, (B) pure silica material **blank-SiO$_2$**: (I) N_2 adsorption–desorption isotherm, (II) mesopore distribution (BJH method, Adsorption Branch), (III) micropore distribution (HK method) and (IV) powder small-angle X-ray diffraction pattern.

particle size after calcination is noticeable, since some degree of particle sintering is commonly observed at this stage of material activation. For comparison, when a similar calcination is used to remove quantitatively template and ligands in the material with NP located in the pores of the silica matrix **Pt@{pores}SiO$_{2\text{-crude}}$**, a limited increase in the nanoparticle size in the final material **Pt@{pores}SiO$_2$** is observed (from 2 nm in the crude to *ca.* 3.5 nm in the calcined) [17]. The embedding of the NP inside the walls of **Pt@{walls}SiO$_2$**, shown by their resistance to leaching and observed by HRTEM, explains this noticeable absence of sintering.

The chemical nature of the nanoparticles – core and surface – in the final material **Pt@{walls}SiO$_2$** was investigated by XPS spectroscopy. The Pt 4f XPS spectrum of **Pt@{walls}SiO$_2$** presented several signals that can be decomposed into two doublets (see SI – Fig. S6 and Table S1): (i) one major doublet associated with the platinum(0) 4f7/2–4f5/2 doublet (signals at 71.1 and 74.25 eV) and (ii) one minor doublet with a binding energy-shift of 1.5 eV toward higher energies (respectively 72.6 eV and 75.75 eV), attributed to Pt—Si species [17]. The ensuing estimate of the relative atomic ratio Pt—Si/Pt—Pt = 0.3, which corresponds to Si/Pt$_{surf}$ = 0.6 [29], is in good agreement with the XPS data of Pt colloids stabilized by octylsilane ligands recently reported [17,24]. Therefore, albeit the material **Pt@{walls}SiO$_2$** was synthesized in water and further calcinated under dry air, which could have lead to metal oxidation, the nanoparticles embedded inside the walls of **Pt@{walls}SiO$_2$** are substantially under their reduced Pt(0) form. The catalytic activity of **Pt@{walls}SiO$_2$** in styrene and propene hydrogenation also goes in that sense.

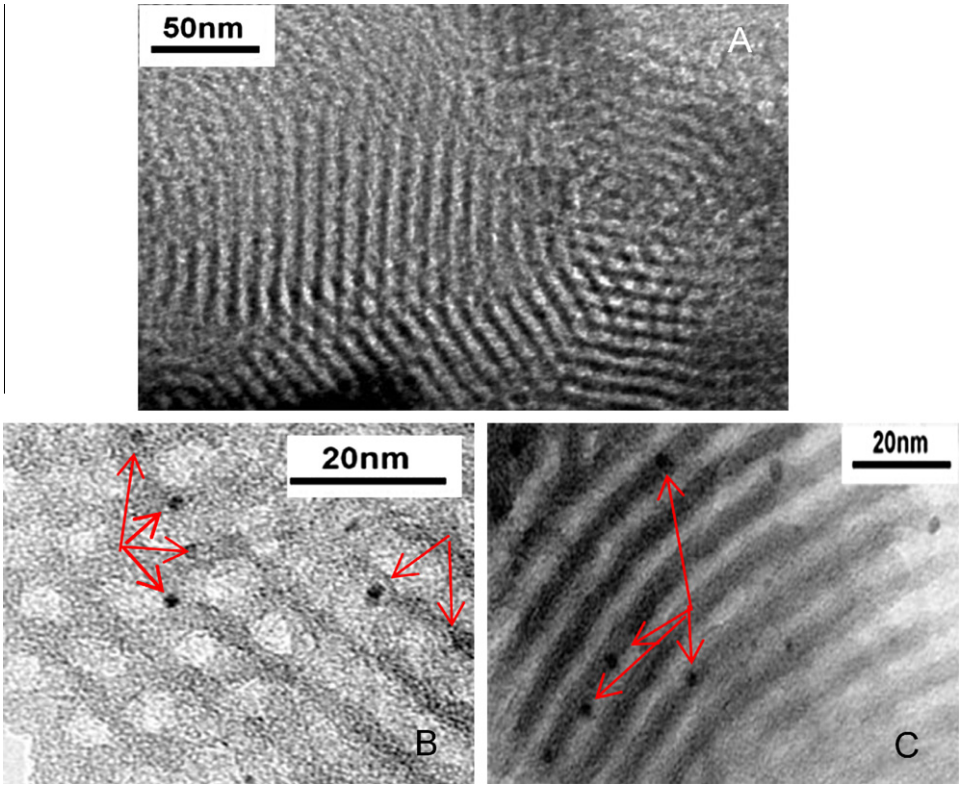

Fig. 4. HRTEM micrographs of the material **Pt@{walls}SiO$_2$** showing (A) the long-range ordering of the pore channels; (B) the honeycomb arrangement of the pore channels and platinum NPs inside the walls and (C) longitudinal arrangement of the pore channels and platinum NPs inside the walls.

3.1.3. Step 2 for the material containing Pt NPs both in the pores and in the walls, ***Pt@{walls + pores}SiO$_2$****: Preparation and characterization*

The protocol outlined above for the selective localization of NP inside the walls of an ordered silica matrix was adapted to a mixture of THF colloidal solutions of hydrophilic **Pt—Cl$_{silane}$** and hydrophobic **Pt—But$_{silane}$** nanoparticles to yield a material having NPs both in the walls and in the pores, **Pt@{walls + pores}SiO$_2$**. The material **Pt@{walls + pores}SiO$_2$** exhibited a high mesoporosity [surface area = 870 m^2/g with 330 m^2/g of micropores (*t*-plot calculation), Dp$_{mesopores}$ = 7 nm (calculated from the Barrett–Joyner–Halenda (BJH) method at the isotherm adsorption branch) and Dp$_{micropores}$ = 1 nm (using Horvath Kavazoe (HK) method)] and a long-range ordering of the pore channels. The complete incorporation of the Pt NPs was observed (0.6 wt.% Pt). The nanoparticles resulted regularly distributed both in its pores and inside its walls (see TEM, HRTEM and Bright Field and High-Angle Annular Dark Field Scanning Transmission Electron Microscopy, BF-STEM and HAADF-STEM, micrographs in Fig. 5 and small-angle X-ray diffraction pattern in SI, Fig. S7). The HAADF-STEM micrograph is best suited to observe the already discussed size difference between the NPs inside the walls and the NPs in the pores. After calcination, the NPs inside the walls kept their native diameter (2 nm), while the NPs in the pores appeared slightly increased as already observed for **Pt@{pores}SiO$_2$** [17].

3.2. Catalytic tests

3.2.1. Propene hydrogenation

The catalytic performances of **Pt@{walls}SiO$_2$** were tested in the classical benchmark catalytic reaction of propene hydrogenation in a continuous tubular reactor and further compared to two reference catalysts. The first reference catalyst was a commercially available **Pt/Al$_2$O$_3$** catalyst consisting of small platinum nanoparticles similar by size and loading (1.8 nm diameter, Pt loading = 0.3 wt.%) to those present in **Pt@{walls}SiO$_2$**, but with platinum particles dispersed over a non-porous alumina surface rather than embedded inside the walls of the highly ordered silica matrix. The second reference catalyst was our previously reported catalyst containing similar Pt nanoparticles located in the pores **Pt@{pores}SiO$_2$** [17] rather than embedded inside the walls of same silica matrix.

Since propene hydrogenation reaction is very fast when using platinum catalysts, preliminary catalytic tests were performed to confirm that we were in a chemical regime and not limited by mass transfer phenomena: the results (see SI – Figs. S8–S10) showed that (i) at constant catalyst loading, the conversion increased linearly with the reverse space velocity, (ii) with a constant flow rate, an increase in the catalyst loading (5, 10 and 30 mg) led to a linear increase in the propene conversion and (iii) the use of a grounded or a non-grounded catalysts led to identical results.

Following the standard test conditions described in materials and methods, thus ascertained to be under chemical regime, the material **Pt@{walls}SiO$_2$** displayed superior catalytic performances with respect to both our reference catalysts, **Pt/Al$_2$O$_3$**, and **Pt@{pores}SiO$_2$**, with turnover frequency per surface Pt atoms (Pt$_{surface}$) in propene hydrogenation twice those of the other two systems (viz. 2.3 s^{-1} vs. respectively, 0.92 s^{-1} and 0.90 s^{-1} – see Fig. 6).

Firstly, these results confirm that the presence of Si atoms on the metal nanoparticles in the ordered materials does not prevent the access to the platinum surface, the TOF of **Pt@{pores}SiO$_2$** and **Pt@{walls}SiO$_2$** being equal or superior to that of the classical **Pt/Al$_2$O$_3$** catalyst.

Secondly, a novel datum appears since **Pt@{walls}SiO$_2$** is a faster hydrogenation catalyst than **Pt@{pores}SiO$_2$**. Since propene hydrogenation on Pt NPs is known to be structure-insensitive at low temperature and for small NPs (i.e. <3 nm) [30], we attribute the increase in TOF observed when the nanoparticles are embedded

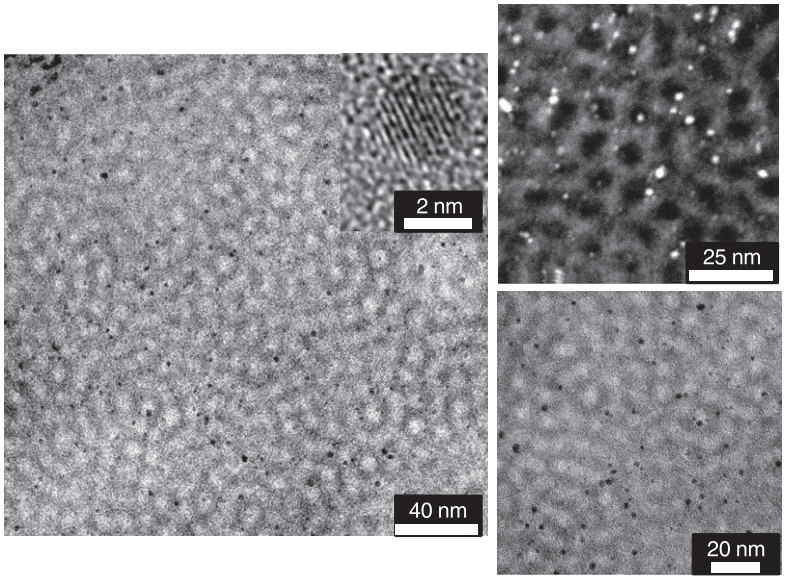

Fig. 5. TEM (left), HRTEM (left inset) and STEM (HAADF, top right and BF, bottom right) micrographs of the material containing Pt nanoparticles in its pores and walls, **Pt@{walls + pores}SiO_2**.

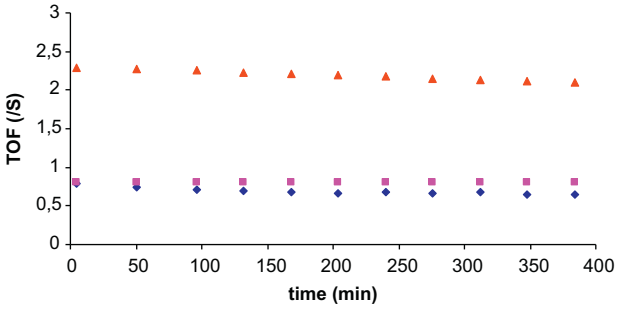

Fig. 6. Plot of TOF (s^{-1}) per surface Pt atoms vs. reaction time (min) for catalysts **Pt@{walls}SiO_2** (red triangles), **Pt@{pores}SiO_2** (pink squares) and **Pt/Al_2O_3** (blue diamonds) in the hydrogenation of propene under dynamic flow reactor. (For interpretation of the references to color in this figure legend, the reader is referred to the web version of this article.)

in the walls of the silica matrix (rather than deposited in its pores or on a non-porous support) to the selective adsorption/capillary condensation of propene in the wall micropores, which increases the coverage of propene on the NPs surface.

Experiments of propene adsorption in the conditions of the catalytic studies for **Pt@{walls}SiO_2**, for **Pt/Al_2O_3** and for **blank-SiO_2** (the homologous platinum-free ordered silica material obtained by reproducing the **Pt@{walls}SiO_2** protocol in the absence of platinum colloid in the THF solution, *vide supra*) were carried out. The experiments showed that while the non-porous support leads to little propene adsorption, the capillary condensation of propene in the micropores of both ordered silica matrices is substantially higher (see SI, Fig. S11), a phenomenon already reported on SBA-15 type solids [31]. No selective adsorption of propene was detected in the mesopore channels, in agreement with the smaller TOF measured for **Pt@{pores}SiO_2** than for **Pt@{walls}SiO_2**.

Catalytic tests of propene hydrogenation have also been used to further prove the selective localization of the NPs inside the silica walls. As already discussed, we prepared **Pt@{walls}$SiO_{2\text{-extract}}$** following a rigorously equal preparation as **Pt@{walls}SiO_2** except for the template removal step (Soxhlet extraction instead of calcination). The less efficient Soxhlet method leaves part of micropores blocked by surfactant, as shown by the microporous volumes (97 vs. 316 m^2/g). When **Pt@{walls}$SiO_{2\text{-extract}}$** is used as catalyst for propene hydrogenation, the TOF drops to about a third (0.8 s^{-1} per $Pt_{surface}$) with respect to TOF with the calcined solid **Pt@{walls}SiO_2** (2.3 s^{-1}), which is by the same 0.3:1 ratio existing between their microporous volumes.

3.2.2. Styrene hydrogenation

The accessibility of Pt nanoparticles located inside the walls of the silica matrix was further assessed by the successful hydrogenation of a hindered substrate such as styrene (see Fig. 7).

The styrene hydrogenation was performed at room temperature in a batch reactor with a substrate/platinum ratio of ca. 4300 for both catalysts, corresponding to a styrene/$Pt_{surface}$ ratio of 10,000 for **Pt@{walls}SiO_2** and of 5000 for **Pt/Al_2O_3**. **Pt/Al_2O_3** is considered as an appropriate reference heterogeneous catalyst because the Pt NPs are supported on non-porous alumina and they are fully accessible. Therefore, the comparison of the catalytic activity of **Pt@{walls}SiO_2** vs. **Pt/Al_2O_3** will give a quantitative estimate of whether the accessibility to the Pt NPs by sizeable molecules such as styrene is diminished when the NPs are embedded inside siliceous walls. Styrene was fully and selectively converted into ethylbenzene within 60 min with similar kinetics for both catalysts. The catalytic activity of **Pt@{walls}SiO_2** in styrene hydrogenation is also very similar to that recently reported for a matrix-free

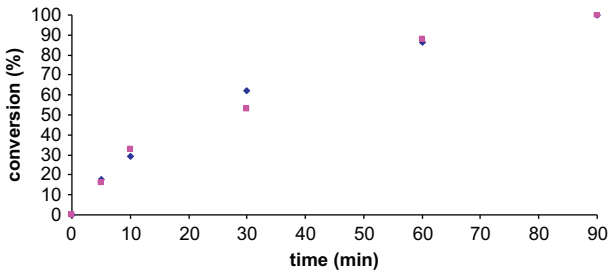

Fig. 7. Plot of conversion (%) vs. time (min) in the hydrogenation of styrene into ethylbenzene at room temperature in batch reactor catalyzed by **Pt/Al_2O_3** (blue diamonds) and by the material containing Pt NPs inside the walls, **Pt@{walls}SiO_2** (pink square) ($R_{Styrene}/Pt_{surface} \sim 5000$ for **Pt/Al_2O_3** and $R_{Styrene}/Pt_{surface} \sim 10{,}000$ for **Pt@{walls}SiO_2**). (For interpretation of the references to color in this figure legend, the reader is referred to the web version of this article.)

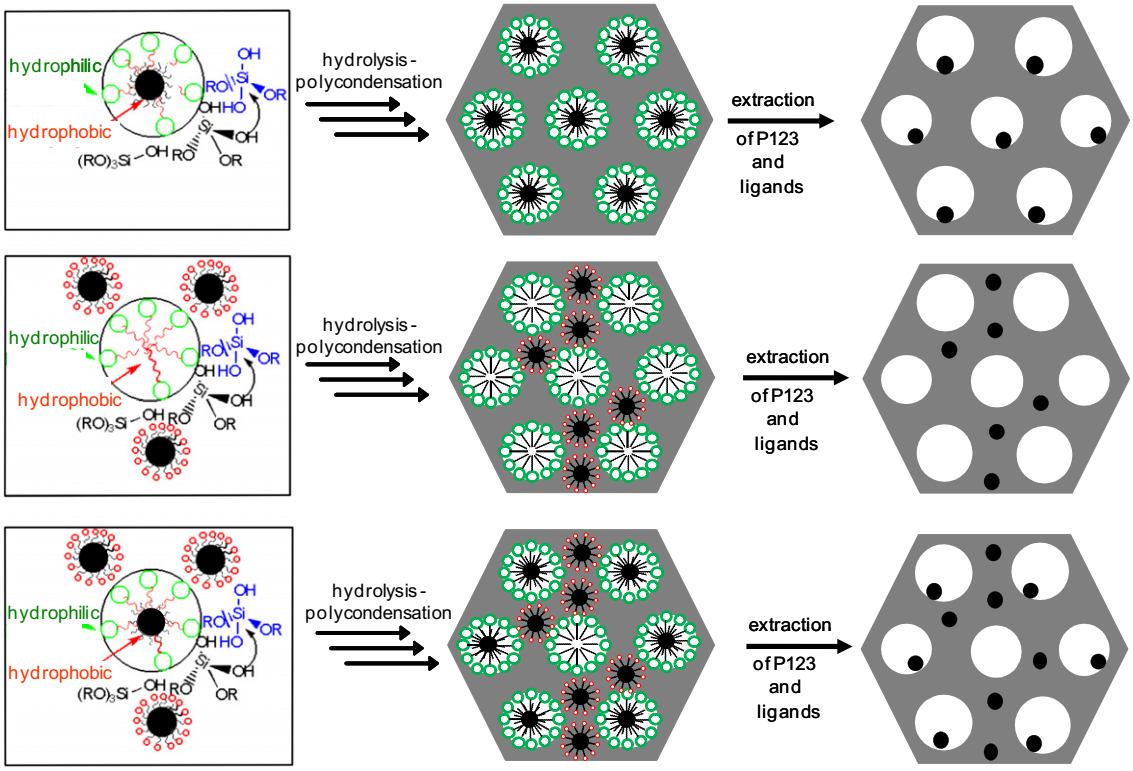

Scheme 1. Principle of metal nanoparticle localization by design in the pores (first line), inside the walls (second line), or both inside the walls and in the pores (third line) of an ordered silica matrix: localization of the preformed nanoparticles in the surfactant mesophases during the sol–gel process (first column) governs the localization of the nanoparticles in final highly structured silica (last column). Three cases are shown: *1st line*: hydrophobic preformed nanoparticles designed to enter the core micelle end up in the pores of the material **M@{pores}SiO_2** (e.g., M = Pt [17]). *2nd line*: hydrophilic preformed nanoparticles designed to be dispersed in the aqueous phase during the sol–gel process end up inside the walls of the material, **M@{walls}SiO_2** (e.g., M = Pt, this work). *3rd line*: mix of hydrophilic and hydrophobic nanoparticles lead to NP localization in both walls and pores **M@{walls + pores}SiO_2** (e.g., M = Pt, this work). The network of micropores present throughout the walls of the materials and that make the embedded NP accessible to reactant during catalysis is not drawn for clarity.

colloidal solution of preformed nanoparticles **Pt—Oct$_{silane}$** [24]. The catalytic activity of the catalyst containing Pt nanoparticles inside the walls, **Pt@{walls}SiO_2**, was therefore found to be as good as silica-free nanoparticles and to be twice as good as the reference heterogeneous catalyst **Pt/Al_2O_3** (TOF = 5.5 s^{-1} at 10 min of reaction for **Pt@{walls}SiO_2** vs. 2.5 s^{-1} for **Pt/Al_2O_3**). These experimental results clearly indicate the easy access of the substrate to the wall-embedded Pt nanoparticles *via* the meso- and micropore channels of the silica framework. We have no current explanation for the surprisingly high catalytic performances of our solid **Pt@{walls}SiO_2** compared with those of the industrial reference heterogeneous catalyst **Pt/Al_2O_3**.

4. Conclusions

This work reported two original syntheses leading to the selective and regular localization of small (2 nm) Pt(0) nanoparticles either inside the walls or both in the pores and inside the walls of mesostructured silica matrices, **Pt@{walls}SiO_2** and **Pt@{walls + pores}SiO_2**. The extensive characterization of the materials (elemental analyses, IR, HRTEM, STEM, SAXS, WAXS, XRD, XPS, N_2 adsorption/desorption, H_2 chemisorption, etc.) confirms the quality of the material structuration and the nature, size and localization of the metal nanoparticles.

The guiding principles to achieve the NPs localization inside the walls during the syntheses have been the following (see scheme 1):

(i) Switch the chemical nature of the preformed nanoparticles from hydrophobic [17] to hydrophilic in order to direct their dispersion into the aqueous phase during the sol–gel process and hence direct them inside the walls of the final material rather than toward the pores.

(ii) Establish a bond between the NPs and their ligand strong enough to prevent exchange with the templating agent, which would confer dispersion in the organic phase and hence disrupt the precise location of the NPs (thus excluding synthetic strategies for material design implying nanoparticles with exchangeable ligands such as ammonium [15]).

(iii) Ensure a sufficient microporosity of the final material by identifying adequate ligands in the preformed NPs and adequate template removal routes from the crude material, to ensure accessibility of the wall-embedded NPs in the final material (hence excluding synthetic routes implying "sticky" ligands such as PVP that can hardly be removed from the final material even after intensive calcinations [16]).

In particular, the syntheses have relied on the development of novel hydrophilic platinum nanoparticles with covalent Pt—Si bonds, **Pt—Cl$_{silane}$**. The hydrophilicity of such NPs is distinctively different from that of the already reported nanoparticles of reduced metals, which are mostly hydrophobic, while the strong Pt—Si interaction prevented exchanges with the surfactant or with the evolved alcohol during the sol–gel process, exchanges which would have drastically modified the hydrophilicity of the NPs. This permanent hydrophilicity excluded the entrance of the metal NPs in the hydrophobic core of the surfactant throughout the synthesis, therefore directing their subsequent localization inside the walls of the inorganic matrix.

In order to prove the full accessibility to the nanoparticles and to start probing the catalytic potential of the materials, we have

tested material **Pt@{walls}SiO_2** in hydrogenation reactions. The chosen reactions were styrene and propene hydrogenations that are not very challenging per se but work well as proof-of-concept benchmark tests. Indeed, the regular distribution of the nanoparticles and their selective localization inside the walls increased the material stability toward nanoparticle leaching and sintering with respect to other siliceous catalysts. The catalytic performances of **Pt@{pores}SiO_2** in propene and styrene hydrogenation are equal or superior to comparable reference catalysts, viz. the analogous mesostructured silica-based material with NPs exclusively in the mesopores, **Pt@{pores}SiO_2**, or the industrial and commercially available **Pt/Al_2O_3** catalyst containing Pt NPs dispersed on non-porous alumina surface, while still not competing with the best systems available that rely on strong metal-support interactions. Applications in more challenging reactions such as selectivity-driven ones or high-temperature reactions, for which sintering is a recognized limitation (e.g., catalytic oxidation in car exhaust treatments), are planned. At this stage, the catalytic results confirm that (i) the surface of embedded Pt NPs is completely accessible to the substrates, with no detrimental effect due to residual impurities on the Pt NPs surface after calcination and (ii) **Pt@{pores}SiO_2** has potential as catalytic material. Given its well-defined nature, our catalytic material appears suitable to help derive precise structure–performance relationships in order to address fundamental questions: deactivation of industrial catalysts, effect of localization on activity, etc., for example through advanced *in situ* mechanistic investigation during catalysis [32,33].

We have shown that the proposed synthetic route can also lead to a material containing NPs both in the walls and in the pores, **Pt@{walls + pores}SiO_2**. The aim was to illustrate the larger span of the methodology depicted in Scheme 1. If further developed, for example, to hetero-bimetallic systems (containing simultaneously independent metal nanoparticles selectively located in their pores and inside their walls, [**M@{walls} + M′@{pores}]SiO_2**), such methodology could also find original catalytic applications such as in cascade reactions with a single catalytic material. Such sophisticated application could justify the extra costs associated with this novel "build-the-bottle-around-the-ship" approach and the necessary study in engineering-related issues (intrinsic kinetic, mass/heat transfer, etc.).

In summary, we have reported two novel catalytic materials **Pt@{walls}SiO_2** and **Pt@{walls + pores}SiO_2** stemming from the same common methodology (see Scheme 1) already applied for analogue **Pt@{pores}SiO_2** [17]. The three materials contain small (ca. 2–3 nm) crystalline Pt(0) nanoparticles localized by design in the desired site of the silica matrix and are active catalysts in benchmark hydrogenation reactions. While the possibility of localizing preformed catalytically active nanoparticles of reduced metals in the pores of silica matrix by a "build-the-bottle-around-the-ship" approach was already known [12–17], this work extends such control toward walls and shows how both localizations can be achieved simultaneously.

Acknowledgments

We would like to thank the French Government of Research for financial support and Dr. M. Aouine, IRCELYON, Villeurbanne (France) for STEM micrographs. CT and EAQ are also very grateful to Prof. A. Corma for insightful suggestions.

Appendix A. Supplementary data

Supplementary data associated with this article can be found, in the online version, at doi:10.1016/j.jcat.2011.09.003.

References

[1] Z. Konya, E. Molnar, G. Tasi, K. Niesz, G.A. Somorjai, I. Kiricsi, Catal. Lett. 113 (2007) 19–28.
[2] A. Goguet, D. Schweich, J.P. Candy, J. Catal. 220 (2003) 280–290.
[3] S. Chytil, W.R. Glomm, I. Kvande, T. Zhao, J.C. Walmsley, E.A. Blekkan, Top. Catal. 45 (2007) 93–99.
[4] C.-J. Jia, F. Schueth, Phys. Chem. Chem. Phys. 13 (2011) 2457–2487.
[5] L. De Rogatis, M. Cargnello, V. Gombac, B. Lorenzut, T. Montini, P. Fornasiero, ChemSusChem 3 (2010) 24–42.
[6] G.A. Somorjai, J.Y. Park, Top. Catal. 49 (2008) 126–135.
[7] C.-M. Yang, B. Zibrowius, W. Schmidt, F. Schueth, Chem. Mater. 16 (2004) 2918–2925.
[8] I. Yuranov, L. Kiwi-Minsker, P. Buffat, A. Renken, Chem. Mater. 16 (2004) 760–761.
[9] C.-M. Yang, H.-A. Lin, B. Zibrowius, B. Spliethoff, F. Schueth, S.-C. Liou, M.-W. Chu, C.-H. Chen, Chem. Mater. 19 (2007) 3205–3211.
[10] H.-A. Lin, C.-H. Liu, W.-C. Huang, S.-C. Liou, M.-W. Chu, C.-H. Chen, J.-F. Lee, C.-M. Yang, Chem. Mater. 20 (2008) 6617–6622.
[11] E. Besson, A. Mehdi, C. Reye, R.J.P. Corriu, J. Mater. Chem. 19 (2009) 4746–4752.
[12] M. Alvaro, C. Aprile, H. Garcia, C.J. Gomez-Garcia, Adv. Funct. Mater. 16 (2006) 1543–1548.
[13] J. Zhu, Z. Konya, V.F. Puntes, I. Kiricsi, C.X. Miao, J.W. Ager, A.P. Alivisatos, G.A. Somorjai, Langmuir 19 (2003) 4396–4401.
[14] Z. Konya, V.F. Puntes, I. Kiricsi, J. Zhu, J.W. Ager III, M.K. Ko, H. Frei, P. Alivisatos, G.A. Somorjai, Chem. Mater. 15 (2003) 1242–1248.
[15] C. Aprile, A. Abad, H. Garcia, A. Corma, J. Mater. Chem. 15 (2005) 4408–4413.
[16] H. Song, R.M. Rioux, J.D. Hoefelmeyer, R. Komor, K. Niesz, M. Grass, P. Yang, G.A. Somorjai, J. Am. Chem. Soc. 128 (2006) 3027–3037.
[17] M. Boualleg, J.-M. Basset, J.-P. Candy, P. Delichere, K. Pelzer, L. Veyre, C. Thieuleux, Chem. Mater. 21 (2009) 775–777.
[18] A. Corma, H. Garcia, Eur. J. Inorg. Chem. (2004) 1143–1164.
[19] C. Garcia, Y. Zhang, F. DiSalvo, U. Wiesner, Angew. Chem., Int. Ed. 42 (2003) 1526–1530.
[20] J.-Y. Chane-Ching, Heat-Stable Ordered Mesoporous Mesostructured Materials Containing Dispersed Metal Oxide Nanocrystals, 2001, 44 pp.
[21] K. Moseley, P.M. Maitlis, J. Chem. Soc. D. (1971) 1604–1605.
[22] K. Pelzer, B. Laleu, F. Lefebvre, K. Philippot, B. Chaudret, J.P. Candy, J.M. Basset, Chem. Mater. 16 (2004) 4937–4941.
[23] M. Boualleg, K. Guillois, B. Istria, L. Burel, L. Veyre, J.-M. Basset, C. Thieuleux, V. Caps, Chem. Commun. (Cambridge, UK) 46 (2010) 5361–5363.
[24] K. Pelzer, M. Haevecker, M. Boualleg, J.-P. Candy, J.-M. Basset, Angew. Chem., Int. Ed. 50 (2011) 5170–5173.
[25] A. Gibaud, J.F. Bardeau, M. Dutreilh-Colas, M. Bellour, V.V. Balasubramanian, A. Robert, A. Mehdi, C. Reye, R.J. Corriu, J. Mater. Chem. 14 (2004) 1854–1860.
[26] D. Zhao, J. Feng, Q. Huo, N. Melosh, G.H. Frederickson, B.F. Chmelka, G.D. Stucky, Science 279 (1998) 548–552.
[27] Z. Jin, X. Wang, X. Cui, J. Non-Cryst. Solids 353 (2007) 2507–2514.
[28] J.P. Candy, P. Fouilloux, A.J. Renouprez, J. Chem. Soc., Faraday Trans. 1 (76) (1980) 616–629.
[29] R. Van Hardeveld, F. Hartog, Surface Sci. 15 (1969) 189–230.
[30] V.V. Zhivonitko, K.V. Kovtunov, I.E. Beck, A.B. Ayupov, V.I. Bukhtiyarov, I.V. Koptyug, J. Phys. Chem. C 115 (2011) 13386–13391.
[31] B.L. Newalkar, N.V. Choudary, P. Kumar, S. Komarneni, T.S.G. Bhat, Chem. Mater. 14 (2001) 304–309.
[32] M. Rivallan, E. Seguin, S. Thomas, M. Lepage, N. Takagi, H. Hirata, F. Thibault-Starzyk, Angew. Chem., Int. Ed. 49 (2010) 785–789.
[33] S. Thomas, M. Rivallan, M. Lepage, N. Takagi, H. Hirata, F. Thibault-Starzyk, Micropor. Mesopor. Mater. 140 (2011) 103–107.